Gradient-Based Aeroservoelastic Optimization with Static Output Feedback

Bret K. Stanford*
NASA Langley Research Center, Hampton, VA, 23681

Static output feedback considers an optimal low-order feedback matrix which directly connects the sensors to the control inputs. This work demonstrates the numerical techniques needed to compute the analytical gradient of the optimal feedback matrix with respect to design variables, which may then be used for gradient-based optimization. The derivatives are demonstrated for aeroservoelastic optimization under a series of closed-loop gust load alleviation constraints, considering a continuous stochastic gust load applied to a transport vehicle configuration, among other design constraints such as flutter and maneuver loads. The optimal trade-offs between passive load alleviation and active load alleviation for static output feedback are compared with those from full-state feedback, which may be considered an upper-bound for effective sensor-based control.

I. Introduction

Aeroservoelastic optimization can be posed as a coupled plant-controller optimization problem,[1] where structural sizing and planform shape design variables define the aircraft plant model, and are optimized in tandem with control architectural details. The controller, typically exposed to the aircraft via trailing edge articulated control surfaces, may be tasked with maneuver load alleviation (MLA), gust load alleviation (GLA), and active flutter suppression (AFS), among other vehicle-level flight control system (FCS) uses. Active performance improvements via control can alleviate the burden on the plant design variables (i.e., actively shed flight loads allow for reduced structural wing weight), and so the synergy between the two sets of design variables (plant and controller) can be very strong.

Regarding control law design variables, early work in integrated aeroservoelastic optimization utilized pre-assigned transfer functions, and optimized the numerator and denominator coefficients of these functions,[2,3] though the resulting design space may be disjointed. More modern work utilizes optimal control, such as a linear quadratic regulator (LQR), which facilitates multiple control inputs and outputs. In this paradigm, considered in Refs. 4–8, the optimal feedback matrix is found which minimizes a performance function, $\boldsymbol{J}$, given as a linear combination of time-averaged control cost and state cost. Design variables may then include members of the control-weighting matrix and/or the state-weighting matrix.

LQR is numerically convenient, but its reliance on full-state feedback is unrealistic. A popular alternative is the use of a Kalman filter to estimate the full state from a small number of sensors (i.e., linear quadratic Gaussian, LQG); a second alternative is static output feedback (SOF), where an optimal feedback matrix directly connects the available outputs (sensors) to the available inputs. There are drawbacks and advantages to both approaches, as summarized in Ref. 9: LQG enjoys stabilization and robustness guarantees that SOF does not, and the design equations are substantially simpler as well. Specifically, SOF feedback entails the onerous computation of three nonlinearly coupled matrix equations (two of which are Lyapunov equations). On the other hand, SOF controllers are much smaller (LQG controllers have the same order as the aircraft plant), and the structure of the feedback matrix can be easily tuned as needed, which is particularly useful for aircraft control.[9]

SOF control, and its role in integrated aeroservoelastic optimization, is the focus of this work. An overall review of the method is given in Ref. 10, and aeroservoelastic analysis of SOF is demonstrated in Refs. 11–13. Coupled aeroservoelastic optimization via SOF is rare, though an example is seen in Ref. 11. The

*Research Aerospace Engineer, Aeroelasticity Branch, bret.k.stanford@nasa.gov, AIAA Senior Member.

authors of that work utilized gradient-based optimization, with derivatives estimated via finite differencing. This approach severely limits the number of design variables that may be considered, and so the extension demonstrated here is the computation of analytical sensitivities of the SOF controller, and the subsequent gradient-based optimization of a detailed aeroservoelastic transport wing with several hundred structural sizing and control law design variables, considering static maneuver loads, gust loads, and flutter.

II. Aeroservoelastic Analysis and Sensitivities

The linear time invariant system of the dynamic aeroservoelastic model considered here is written as:

$$\dot{\boldsymbol{x}} = \boldsymbol{A} \cdot \boldsymbol{x} + \boldsymbol{B} \cdot \boldsymbol{u} + \boldsymbol{B}_w \cdot w \tag{1}$$

where $\boldsymbol{x}$ is the state vector, $\boldsymbol{u}$ is the commanded input, and w is a zero-mean unit-intensity white noise. Outputs of the system (sensor measurements) are given by:

$$\boldsymbol{y} = \boldsymbol{C} \cdot \boldsymbol{x} \tag{2}$$

The goal is to find a feedback matrix of the form $\boldsymbol{u} = -\boldsymbol{K} \cdot \boldsymbol{y}$ which minimizes the expected value of a performance index:

$$J = \frac{1}{2} \cdot E\left[\int_0^\infty (\boldsymbol{x}^T \cdot \boldsymbol{Q} \cdot \boldsymbol{x} + \boldsymbol{u}^T \cdot \boldsymbol{R} \cdot \boldsymbol{u}) \cdot dt\right] \tag{3}$$

where $\boldsymbol{Q}$ is the state weighting matrix, and $\boldsymbol{R}$ is the control weighting matrix. The equations needed to compute $\boldsymbol{K}$ are not derived here, only the final set is reproduced from Ref. 9. Ignoring the white noise input for the time-being, these equations are:

$$\boldsymbol{A}_c^T \cdot \boldsymbol{P} + \boldsymbol{P} \cdot \boldsymbol{A}_c + \boldsymbol{C}^T \cdot \boldsymbol{K}^T \cdot \boldsymbol{R} \cdot \boldsymbol{K} \cdot \boldsymbol{C} + \boldsymbol{Q} = \boldsymbol{0} \tag{4}$$

$$\boldsymbol{A}_c \cdot \boldsymbol{S} + \boldsymbol{S} \cdot \boldsymbol{A}_c^T + \boldsymbol{I} = \boldsymbol{0} \tag{5}$$

$$\boldsymbol{K} = \boldsymbol{R}^{-1} \cdot \boldsymbol{B}^T \cdot \boldsymbol{P} \cdot \boldsymbol{S} \cdot \boldsymbol{C}^T \cdot \left(\boldsymbol{C} \cdot \boldsymbol{S} \cdot \boldsymbol{C}^T\right)^{-1} \tag{6}$$

where $\boldsymbol{A}_c = \boldsymbol{A} - \boldsymbol{B} \cdot \boldsymbol{K} \cdot \boldsymbol{C}$, the symmetric positive semidefinite matrix $\boldsymbol{P}$ is the solution to the Ricatti equation, and $\boldsymbol{S}$ is a symmetric matrix of Lagrange multipliers. Eqs. 4-6 present a coupled set of nonlinear matrix equations for the unknowns $\boldsymbol{K}$, $\boldsymbol{P}$, and $\boldsymbol{S}$, the first two of which are Lyapunov equations.

A combination of algorithms is used in this work to solve the SOF equations. First, a gradient-based optimization (with each member of $\boldsymbol{K}$ as a design variable) is used to minimize the performance index J of Eq. 3, with the constraint that $\boldsymbol{A}_c$ must be stable. This algorithm pushes the solution into the correct region, but is unable to efficiently drive the residual of Eq. 6 to machine-zero. As such, this first algorithm is then followed, after a fixed number of iterations, by the well-known Moerder-Calise algorithm,[14] which uses a recurring Newton update to compute $\boldsymbol{K}$. Care must be taken in this algorithm to limit the step size to $\boldsymbol{K}$, such that $\boldsymbol{A}_c$ remains stable: an unstable $\boldsymbol{K}$ will destabilize the algorithm.

Having computed the optimal feedback matrix, the closed-loop response of the aeroservoelastic system to the input gust w is computed via another Lyapunov equation:

$$\boldsymbol{A}_c \cdot \boldsymbol{X} + \boldsymbol{X} \cdot \boldsymbol{A}_c^T + \boldsymbol{B}_w \cdot U_\sigma^2 \cdot \boldsymbol{B}_w^T = \boldsymbol{0} \tag{7}$$

where $\boldsymbol{X}$ is the state covariance matrix, and U_σ is the design gust velocity.[15] Gust-based performance metrics, exposed to the aeroservoelastic optimizer in the form of design constraints, are then written as $g(\boldsymbol{X})$.

In order to conduct this optimization under a large number of design variables, gradient-based optimization is required, with the gradients computed in an analytical manner. With design variables grouped into the vector $\boldsymbol{q}$, the derivatives of the gust metrics g are written as:

$$\frac{dg}{d\boldsymbol{q}} = \frac{dg}{d\boldsymbol{X}} \cdot \frac{d\boldsymbol{X}}{d\boldsymbol{q}} \tag{8}$$

Ideally, analytical derivative computations will have a cost which scales nearly-independently of the number of design variables in $\boldsymbol{q}$: see for example, adjoint computations for linear and nonlinear algebraic systems of equations, or eigenvalue derivatives.[16] Derivatives of Lyapunov equations, on the other hand, scale poorly with the number of design variables, as one additional Lyapunov equation must be solved per design variable of interest.[17] For example, the covariance derivative needed in Eq. 8 is computed as:

$$\boldsymbol{A}_c \cdot \frac{d\boldsymbol{X}}{d\boldsymbol{q}} + \frac{d\boldsymbol{X}}{d\boldsymbol{q}} \cdot \boldsymbol{A}_c^T + \frac{d\boldsymbol{A}_c}{d\boldsymbol{q}} \cdot \boldsymbol{X} + \boldsymbol{X} \cdot \frac{d\boldsymbol{A}_c^T}{d\boldsymbol{q}} = \boldsymbol{0} \tag{9}$$

where it has been assumed that $\boldsymbol{B}_w$ is not dependent upon the design variables. The closed-loop plant derivatives are given as:

$$\frac{d\boldsymbol{A}_c}{d\boldsymbol{q}} = \frac{d\boldsymbol{A}}{d\boldsymbol{q}} - \frac{d\boldsymbol{B}}{d\boldsymbol{q}} \cdot \boldsymbol{K} \cdot \boldsymbol{C} - \boldsymbol{B} \cdot \frac{d\boldsymbol{K}}{d\boldsymbol{q}} \cdot \boldsymbol{C} - \boldsymbol{B} \cdot \boldsymbol{K} \cdot \frac{d\boldsymbol{C}}{d\boldsymbol{q}} \tag{10}$$

Eq. 10 requires the derivatives of the feedback matrix, which is the focus of this work. Just as the derivative of a standard Lyapunov equation requires one additional Lyapunov equation per design variable, the derivative of the SOF systems (Eqs. 4-6) analogously requires the solution of a coupled set of nonlinear matrix equations, for each design variable. These three equations are:

$$\begin{aligned}\boldsymbol{A}_c^T \cdot \frac{d\boldsymbol{P}}{d\boldsymbol{q}} + \frac{d\boldsymbol{P}}{d\boldsymbol{q}} \cdot \boldsymbol{A}_c + \frac{d\boldsymbol{A}_c^T}{d\boldsymbol{q}} \cdot \boldsymbol{P} + \boldsymbol{P} \cdot \frac{d\boldsymbol{A}_c^T}{d\boldsymbol{q}} + \left(\frac{d\boldsymbol{C}^T}{d\boldsymbol{q}} \cdot \boldsymbol{K}^T + \boldsymbol{C}^T \cdot \frac{d\boldsymbol{K}^T}{d\boldsymbol{q}}\right) \cdot \boldsymbol{R} \cdot \boldsymbol{K} \cdot \boldsymbol{C} + \\ \boldsymbol{C}^T \cdot \boldsymbol{K}^T \cdot \frac{d\boldsymbol{R}}{d\boldsymbol{q}} \cdot \boldsymbol{K} \cdot \boldsymbol{C} + \boldsymbol{C}^T \cdot \boldsymbol{K}^T \cdot \boldsymbol{R} \cdot \left(\frac{d\boldsymbol{K}}{d\boldsymbol{q}} \cdot \boldsymbol{C} + \boldsymbol{K} \cdot \frac{d\boldsymbol{C}}{d\boldsymbol{q}}\right) + \frac{d\boldsymbol{Q}}{d\boldsymbol{q}} = \boldsymbol{0}\end{aligned} \tag{11}$$

$$\boldsymbol{A}_c \cdot \frac{d\boldsymbol{S}}{d\boldsymbol{q}} + \frac{d\boldsymbol{S}}{d\boldsymbol{q}} \cdot \boldsymbol{A}_c^T + \frac{d\boldsymbol{A}_c}{d\boldsymbol{q}} \cdot \boldsymbol{S} + \boldsymbol{S} \cdot \frac{d\boldsymbol{A}_c^T}{d\boldsymbol{q}} = \boldsymbol{0} \tag{12}$$

$$\begin{aligned}\frac{d\boldsymbol{K}}{d\boldsymbol{q}} = \boldsymbol{R}^{-1} \cdot \left(\left(-\frac{d\boldsymbol{R}}{d\boldsymbol{q}} \cdot \boldsymbol{K} \cdot \boldsymbol{C} - \boldsymbol{R} \cdot \boldsymbol{K} \cdot \frac{d\boldsymbol{C}}{d\boldsymbol{q}}\right) \cdot \boldsymbol{S} \cdot \boldsymbol{C}^T - \boldsymbol{R} \cdot \boldsymbol{K} \cdot \boldsymbol{C} \cdot \left(\frac{d\boldsymbol{S}}{d\boldsymbol{q}} \cdot \boldsymbol{C}^T + \boldsymbol{S} \cdot \frac{d\boldsymbol{C}^T}{d\boldsymbol{q}}\right) + \right. \\ \left. \left(\frac{d\boldsymbol{B}^T}{d\boldsymbol{q}} \cdot \boldsymbol{P} + \boldsymbol{B}^T \cdot \frac{d\boldsymbol{P}}{d\boldsymbol{q}}\right) \cdot \boldsymbol{S} \cdot \boldsymbol{C}^T + \boldsymbol{B}^T \cdot \boldsymbol{P} \cdot \left(\frac{d\boldsymbol{S}}{d\boldsymbol{q}} \cdot \boldsymbol{C}^T + \boldsymbol{S} \cdot \frac{d\boldsymbol{C}^T}{d\boldsymbol{q}}\right)\right) \cdot \left(\boldsymbol{C} \cdot \boldsymbol{S} \cdot \boldsymbol{C}^T\right)^{-1}\end{aligned} \tag{13}$$

Solution of Eqs. 11-13 yields the derivatives of $\boldsymbol{P}$, $\boldsymbol{S}$, and $\boldsymbol{K}$ with respect to $\boldsymbol{q}$, the latter of which is needed in Eq. 10, and is accomplished with the same linearized update algorithm (i.e., Moerder-Calise[14]) used for the original SOF controller (Eqs. 4-6). Convergence of the derivative Eqs. 11-13 can be more aggressive, however, since the Lyapunov matrix driver ($\boldsymbol{A}_c$) is frozen in Eqs. 11 and 12, and so there is no worry that overly-large step sizes will destabilize the system. This is in contrast with the original SOF equations, where $\boldsymbol{A}_c$ is part of the solution process, and so care must be taken not to obtain an unstable closed-loop system. Despite this, the overall cost of computing the derivative of $\boldsymbol{K}$ is very high, since these coupled nonlinear matrix sensitivity equations must be solved for each design variable independently, though the independent operations can be done in parallel.

III. Optimization Test Case

The demonstration case considered here is a metallic wingbox of the Common Research Model,[18] a generic swept-wing subsonic transport configuration with an aspect ratio of nine. The optimization desires to identify the configuration with the lowest structural mass, which can still withstand the static maneuver loads and gust loads (both with and without the assistance of twenty trailing edge control surfaces distributed from root to tip) and also remain flutter-free. Detailed information regarding this optimization problem can be found in Ref. 19; only cursory details are provided here. Three types of design variables are considered by the gradient-based optimizer:

1. Structural sizing: the skin panels, ribs, and spar sections of the wingbox are discretized into design patches with smeared stiffeners. The shell thickness, stiffener thickness, and stiffener height is optimized separately for each design patch.

2. Maneuver load alleviation: the optimizer dictates the static deflection of each control surface across two closed-loop static aeroelastic maneuver loads ($-1g$ and $2.5g$). Two additional open-loop maneuver loads are applied without the use of MLA as well, which the optimizer must satisfy passively using the sizing variables alone.
3. Gust load alleviation: the members of the diagonal matrix $\boldsymbol{R}$ are utilized as design variables as well (one per control surface), and used to generate a feedback matrix $\boldsymbol{K}$ (where $\boldsymbol{Q}$ is frozen throughout the optimization, and the output term $\boldsymbol{C}$ is based on six accelerometers distributed throughout the wing). This control architecture in turn dictates the closed-loop gust response. As with the static maneuver loads, an open-loop gust load is applied as well, which the optimizer must satisfy passively using the sizing variables alone.

Several categories of design constraints must be satisfied during the optimization process:

1. Static stresses: during each maneuver load (both open-loop, and closed-loop via MLA), the stresses of each wingbox finite element must be within the failure envelope.
2. Static buckling: during each maneuver load, the buckling factor of each stiffened panel must be within the failure envelope.
3. Flutter: the airplane must be free of instability up to 15% of the dive speed (i.e., the eigenvalues of $\boldsymbol{A}$ must be in the left-half-plane).
4. Dynamic stresses: during the continuous gust load (both open-loop, and closed-loop via GLA), the equal-probability stress hypersurface[20] of each wingbox finite element must be within the failure envelope.
5. Dynamic buckling: during the continuous gust load, the equal-probability buckling hypersurface of each stiffened panel must be within the failure envelope.
6. Control surface RMS rate: during the closed-loop continuous gust, the RMS rate of each control surface must be less than some acceptable rate limit.

Constraint-aggregation[21] is used to reduce the number of constraints to an acceptable level, for each of these categories.

The dynamic stress, buckling, and RMS rate constraints are examples of g from Eq. 8, which requires derivatives with respect to $\boldsymbol{q}$ (sizing and control law variables, in this case: MLA variables are grouped within $\boldsymbol{q}$ as well, but have no impact on the gust problem). The derivatives are computed via Eqs. 9-13, where the plant $\boldsymbol{A}$ is a function of the sizing variables, $\boldsymbol{B}$ and $\boldsymbol{C}$ are assumed independent of design variables, and $\boldsymbol{R}$ is in fact identical to the control law design variables (and so the pertinent $\boldsymbol{R}$ derivative is the identity matrix). A modal analysis is used to define $\boldsymbol{A}$, where the solution vector $\boldsymbol{x}$ contains the structural modal amplitudes and their time derivatives, aerodynamic lag states via a rational function approximation, control surface aerodynamic terms and their lag states, third-order actuator modeling terms, gust column aerodynamic lag terms, and gust forming filter terms. More details are given in Ref. 19.

The effectiveness of the GLA controller is driven by the tension between the dynamic stress/buckling constraints, and the control surface RMS rate constraints. If the allowable rotation rate is set to a high limit, this RMS constraint becomes inactive, and the optimizer is easily able to find a combination of $\boldsymbol{R}$ values which will satisfy the closed-loop gust-based stress and buckling constraints. On the other hand, if the RMS limit is set to a low value (active constraint), this limits the ability of the optimizer to use active control to entirely handle the stress and gust constraints; the optimizer is then forced to passively stiffen the wing, resulting in an increase in structural mass (the objective function). For very-low RMS limits, the controller is entirely incapacitated, and the closed-loop gust load effectively becomes an open-loop load entirely satisfied with sizing design variables. The focus of this work is to trace out this optimal trade-off curve between structural wingbox weight and RMS rate limits.

IV. Results

The aeroservoelastic optimization process here is defined by multiple types of design variables and constraints, and it is of interest to understand the reaction of the optimization system (namely, the increase or decrease in the objective function, structural mass) when these variables and constraints are phased in or out in an isolated manner. A comprehensive study along these lines is given in Ref. 19; the current work is only interested in understanding the effect of introducing the gust constraints (stress, buckling, RMS

rate). A baseline system is obtained if the system is optimized under static loads (with and without MLA) and flutter. If an open-loop gust constraint (stress, buckling) is added, a structural mass penalty (where structural mass is computed based on the volume of the finite element model) of 9.7% is incurred. As noted above, closed-loop GLA control can be used to recover some of this penalty, depending on the location of the imposed RMS constraint.

Prior to discussing these design-oriented issues, however, typical output feedback control results (and their analytical sensitivities) are presented and verified. This is done for the baseline aeroservoelastic design noted previously, where gust constraints have not been applied yet. Convergence of the static output feedback process (Eqs. 4-6) is given in Fig. 1, in terms of the residual norm of Eq. 6, the least-stable eigenvalue (real part) of the closed-loop system $\boldsymbol{A}_c$, and each member of $\boldsymbol{K}$. Both phases of the convergence are shown, as noted above: the first minimizes J across the $\boldsymbol{K}$ parameter space; the second phase uses the Moerder-Calise algorithm.[14]

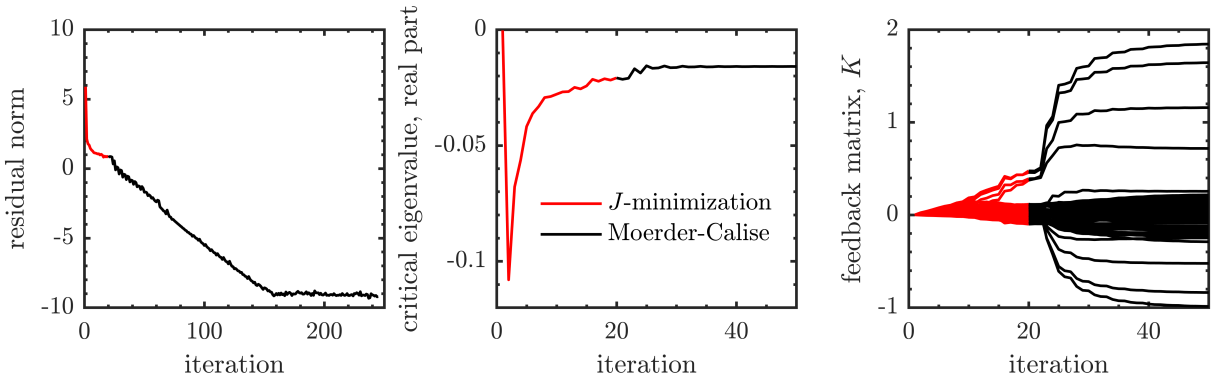

Figure 1. Convergence of the static output feedback matrix.

J-minimization is conducted for 20 iterations, where the residual drops 5 orders-of-magnitude, but then stalls. Moerder-Calise is then able to drop the residual by another 10 orders-of-magnitude, reaching machine-zero after 150 iterations. This phasing of algorithms is generally useful due to the fact that Moerder-Calise requires an initial stabilizing feedback matrix to converge,[9] and the $\boldsymbol{A}_c$-stability constraint applied during the J-minimization process will ensure this requirement is met. This issue is not a concern in this work, however, as the open-loop system ($\boldsymbol{K} = \boldsymbol{0}$) is stable owing to the satisfaction of the flutter constraint, as can be seen in the stable eigenvalue at iteration 0 in Fig. 1. The critical stability of $\boldsymbol{A}_c$ is largely set after the first 20 iterations, though the actual values of $\boldsymbol{K}$ change substantially through iteration 50.

Next, the accuracy of the analytical derivatives computed via Eqs. 9-13 is verified, for the closed-loop system that uses the feedback matrix of Fig. 1. As noted above, dynamic stresses are constrained during the optimization, in the sense that the equal-probability stress hypersurface of each wingbox finite element must be within the failure envelope during the continuous gust. These element-based constraints are aggregated into a single value (to minimize the number of constraints), and the derivative of this final aggregated constraint with respect to each member of the control input $\boldsymbol{R}$, is shown in Fig. 2. The analytical derivatives are compared with finite difference estimates, with generally good agreement. Identifying a good finite difference step size is difficult in general due to competing problems with numerical round-off (small steps) and nonlinear response (large steps), and is particularly problematic here due to the large volume of Lyapunov equation calls. The preferred method of verifying analytical gradients, complex step perturbation,[22] is not possible here due to the inability of the Lyapunov solver to accept complex inputs.

Additional analytical derivatives are shown (without finite difference verification) in Fig. 3. The first contour in the figure show the derivative of the same gust-based stress metric as in Fig. 2, but now with respect to the structural sizing of each wingbox design patch (i.e., shell thickness). The second contour shows a similar result for panel buckling. These two sensitivities are largely localized in nature: the magnitude of the sizing derivatives are highest in the locations of the wingbox with the largest gust-induced loads (in the upper and lower skins, at semispan locations between $2 \cdot y/b$ of 0.6 and 0.75). The third contour in Fig. 3, on the other hand, is the sizing derivative of the closed-loop control surface rotation rate RMS, where the RMS value of each control surface has been aggregated into a single metric, as before.

This third contour plot is more representative of the coupled aeroservoelastic nature of the problem, as

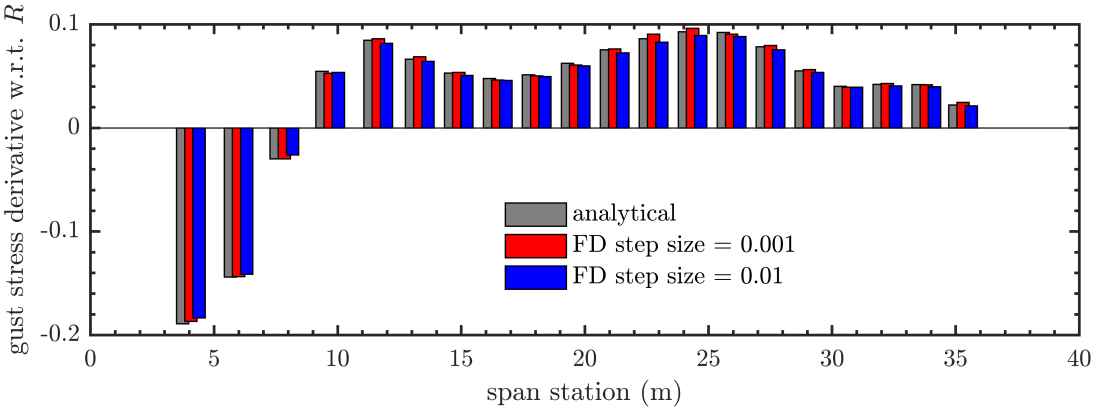

Figure 2. Derivatives of the gust-based stress metric with respect to the control inputs, $\boldsymbol{R}$.

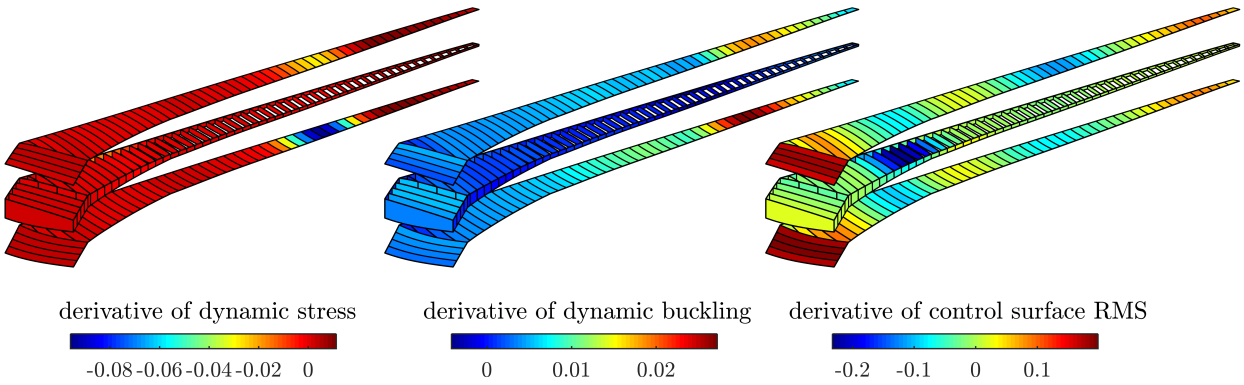

Figure 3. Derivatives with respect to structural wingbox sizing parameters.

structural sizing will impact the plant matrix $\boldsymbol{A}$, which in turn helps shape the optimal SOF feedback matrix $\boldsymbol{K}$, and then finally the covariance of the response, $\boldsymbol{X}$ (which then defines the RMS of each control surface rotation). Given these complex interdependencies, the distribution of sensitivity throughout the wingbox in this third contour in Fig. 2 is spatially heterogeneous and nonintuitive. Certainly the phasing and spatial distribution of each structural mode shape will impact the control effort needed for GLA, and this is reflected in the large negative sensitivities in the rib webs: the engine is attached in this location, and the least-stable aeroelastic mode for this configuration is an engine-driven torsional mode.[19]

Finally, the sensitivities shown above are utilized for a complete aeroservoelastic optimization. Starting with the design noted above, which has a weight penalty of 9.7% and includes an open-loop gust constraint, GLA is implemented along with the closed-loop gust constraints. Fig. 4 traces out the optimal structural mass under changes in the allowable control surface rotation RMS rate. The structural mass penalty varies from 9.7% (where the RMS limit is very small, effectively eliminating the impact of GLA) to 0.8% (where the RMS limit is very large: GLA is then able to alleviate the gust-burden of the wingbox, and therefore reduce structural weight). Most of the gust penalty is recovered in this latter extreme: a non-zero penalty remains only because the system is still forced to satisfy an open-loop gust constraint, with GLA turned off.

The SOF controller in Fig. 4 is compared with an LQR controller based on full-state feedback ($\boldsymbol{C} = \boldsymbol{I}$). The LQR control design and associated sensitivity equations are considerably simpler and less-expensive relative to SOF,[17] and the performance of LQR may be thought of as the best-achievable for a given plant and control input. Given this, the structural mass of the aeroservoelastic system optimized with LQR is consistently lower than that with SOF for a given RMS rate limit constraint: a more effective GLA controller allows for more structural mass to be removed from the wingbox. The largest structural mass difference between the two controllers is a 1.4% penalty, and the difference drops to zero in the limit of very-small allowable RMS rate rotations: both controllers become equally defective under this constraint. The difference

also disappears in the limit of very-large allowable RMS rate rotations, as both controllers have more than enough design freedom to actively alleviate the gust loads.

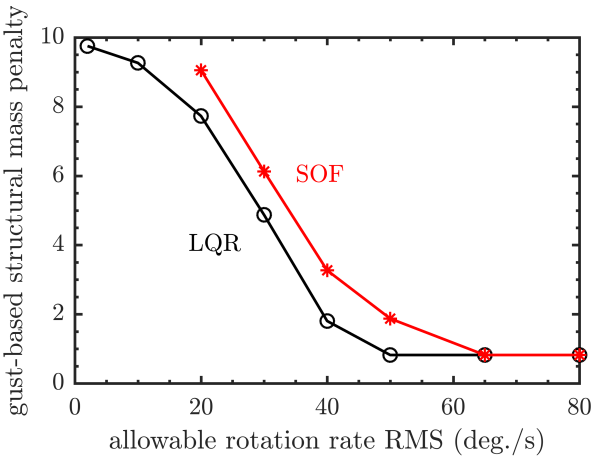

Figure 4. Dependence of optimal structural mass on controller type and control surface rate limits.

V. Conclusions

This work outlines methods for considering static output feedback controllers during integrated gradient-based aeroservoelastic optimization. Static output feedback has benefits relative to other optimal sensor-based feedback algorithms, but suffers from high computational cost and algorithmic complexity. The computational steps required to compute the analytical derivative of the output feedback matrix with respect to design variables are demonstrated here, as are methods to use those derivatives to represent a closed-loop gust-based design constraint. Optimal aeroservoelastic trends (namely, trade-offs between active and passive load allevation) for static output feedback are compared with those from full-state feedback, where the former has a moderately inferior wing structure and control authority layout, owing to the more-realistic sensor-based representation.

Acknowledgments

This work is funded by the NASA Advanced Air Transport Technologies project.

References

[1]Fathy, H., Reyer, J., Papalambros, P., Ulsoy, A., "On the Coupling between the Plant and Controller Optimization Problems," *Proceedings of the American Control Conference*, Arlington, VA, June 25-27, 2001.

[2]Livne, E., Schmidt, A., Friedmann, P., "Integrated Structure/Control/Aerodynamic Synthesis of Actively Controlled Composite Wings," *Journal of Aircraft*, Vol. 30, No. 3, pp. 387-394, 1993.

[3]Livne, E., "Integrated Aeroservoelastic Optimization: Status and Direction," *Journal of Aircraft*, Vol. 36, No. 1, pp. 122-145, 1999.

[4]Layton, J., "Aeroservoelastic Tailoring for Gust Response of a Typical Section Aeroelastic Model," *AIAA Structures, Structural Dynamics, and Materials Conference*, New Orleans, LA, April 10-13, 1995.

[5]Haghighat, S., Martins, J,. Liu, H., "Aeroservoelastic Design Optimization of a Flexible Wing," *Journal of Aircraft*, Vol. 49, No. 2, pp. 432-443, 2012.

[6]Jackson, T., Livne, E., "Integrated Aeroservoelastic Design Optimization of Actively Controlled Strain-Actuated Flight Vehicles," *AIAA Journal*, Vol. 52, No. 6, pp. 1105-1123, 2014.

[7]Stanford, B., "Optimization of an Aeroservoelastic Wing with Distributed Multiple Control Surfaces," *Journal of Aircraft*, Vol. 53, No. 4, pp. 1131-1144, 2016.

[8]Broughton-Venner, J., Wynn, A., Palacios, R., "Aeroservoelastic Optimisation of Aerofoils with Compliant Flaps via Reparameterization and Variable Selection," *AIAA Journal*, Vol. 56, No. 3, pp. 1146-1157, 2018.

[9]Stevens, B., Lewis, F., *Aircraft Control and Simulation*, John Wiley and Sons, Hoboken, NJ, 2003.

[10]Syrmos, V., Abdallah, C., Dorato, P., Grigoriadis, K., "Static Output Feedback - A Survey," *Automatica*, Vol. 33, No. 2, pp. 125-137, 1997.

[11]Nam, C., Kim, Y., "Optimal Design of Composite Lifting Surface for Flutter Suppression with Piezoelectric Actuators," *AIAA Journal*, Vol. 33, No. 10, pp. 1897-1904, 1995.

[12]Patil, M., Hodges, D., "Output Feedback Control of the Nonlinear Aeroelastic Response of a Slender Wing," *Journal of Guidance, Control, and Dynamics*, Vol. 25, No. 2, pp. 302-308, 2002.

[13]Fonte, F., Ricci, S., Mantgazza, P., "Gust Load Alleviation for a Regional Aircraft Through a Static Output Feedback," *Journal of Aircraft*, Vol. 52, No. 5, pp. 1559-1574, 2015.

[14]Moerder, D., Calise, A., "Convergence of a Numerical Algorithm for Calculating Optimal Output Feedback Gains," *IEEE Transactions on Automatic Control*, Vol. AC-30, pp. 900-903, 1985.

[15]Hoblit, F., *Gust Loads on Aircraft: Concepts and Applications*, AIAA, Washington DC, 1988.

[16]Adelman, H., Haftka, R., "Sensitivity Analysis of Discrete Structural Systems," *AIAA Journal*, Vol. 24, No. 5, pp. 823-832, 1986.

[17]Gilbert, M., "An Analytical Sensitivity Method for use in Integrated Aeroservoelastic Aircraft Design," *Mechanical Systems and Signal Processing*, Vol. 4, No. 3, pp. 215-231, 1990.

[18]https://commonresearchmodel.larc.nasa.gov, retrieved October 2018

[19]Stanford, B., "Aeroservoelastic Optimization under Stochastic Gust Constraints," *AIAA Applied Aerodynamics Conference*, Atlanta, GA, June 25-29, 2018.

[20]Engelsen, F., Livne, E., "Quadratic Stress Failure Constraints for Structures under Combined Steady and Random Excitation," *AIAA Journal*, Vol. 42, No. 1, pp. 132-140, 2004.

[21]Kreisselmeier, G., Steinhauser, R., "Systematic Control Design by Optimizing a Vector Performance Index", *International Federation of Active Controls Symposium on Computer-Aided Design of Control Systems*, Zurich, Switzerland, 1979.

[22]Martins, J., Sturdza, P., Alonso, J., "The Complex Step Derivative Approximation", *ACM Transactions on Mathematical Software*, Vol. 29, pp. 245-262, 2003.